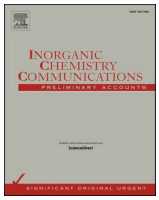
Inorganic Chemistry Communications 191 (2026) 116968



Contents lists available at ScienceDirect

Inorganic Chemistry Communications

journal homepage: www.elsevier.com/locate/inoche



Research Article

Visible-light-driven photocatalytic activity of 2D/1D g-C_3N_4/Bi_2S_3 heterojunction for efficient degradation of ciprofloxacin and methylene blue

Bhuvaneswari Kandasamy [a,*], Balaji Parasuraman [b], Pugazhenthiran Nalandhiran [c], S. Manimegalai [d], Sivaprakash Paramasivam [e], Pazhanivel Thangavelu [b], Ikhyun Kim [e], Jintae Lee [f], Govindasamy Palanisamy [f,*]

[a] Department of Physics, Faculty of Science and Humanities, SRM University Delhi-NCR, Sonepat, Haryana, 131029 India
[b] Smart Material Laboratory, Department of Physics, Periyar University, Salem 636011, Tamil Nadu, India
[c] Laboratorio de Fotoquímica y Fotofísica, Departamento de Química, Universidad Técnica Federico Santa María, Av. España, Valparaíso 1680, Chile
[d] Department of Physics, Vivekanandha College of Engineering for Women (Autonomous), Elayampalayam, Tiruchengode, 637205 Namakkal, Tamilnadu, India
[e] Department of Mechanical Engineering, Keimyung University, Daegu 42601, Republic of Korea
[f] School of Chemical Engineering, Yeungnam University, 280 Daehak-Ro, Gyeongsan 38541, Republic of Korea

ARTICLE INFO

Keywords:
Bi_2S_3:g-C_3N_4 nanocomposite
Photocatalytic degradation, MB
Ciprofloxacin
UV–visible light irradiation

ABSTRACT

Efficiently treating polluted water is crucial for combating waterborne diseases, preserving aquatic species, and ensuring a long-term clean water supply. In this study, we studied the elimination of both dye and drug pollutants using a Bi_2S_3:g-C_3N_4 nanocomposite photocatalyst. The sample structure, functional group, and morphology of the prepared samples were studied using XRD, HRTEM, XPS, FTIR, and UV–Vis. spectroscopy. Bi_2S_3:g-C_3N_4 nanocomposite exhibited higher photocatalytic activity compared to the bare samples. This higher photocatalytic performance may be due to the efficient separation of electron-hole pairs and the enhanced charge-carrier transport. The 2D/2D interface between Bi_2S_3 and g-C_3N_4 provides a large surface area and strong interfacial charge transfer. Moreover, this heterojunction efficiently controls charge recombination by extending the lifetime of the photogenerated carriers. Bi_2S_3:g-C_3N_4 nanocomposite exhibits excellent photocatalytic degradation of organic pollutants such as methylene blue and ciprofloxacin. Based on these results, highlight the strong potential of the Bi_2S_3:g-C_3N_4 nanocomposite for environmentally friendly wastewater treatment applications.

1. Introduction

Water pollution is a dangerous problem for human health and environmental stability. In many industries, such as cosmetics, leather, paper, paint, and the pharmaceutical industries, the use of water sources worldwide [1,2]. These industries directly release the unreacted organic dyes and pigments into the water bodies [3,4]. In particular, the textile industry releases more than 20% of the toxic and non-biodegradable organic compounds into the ecosystem and affects the global water sources [5]. These non-biodegradable compounds not only change the color of water but also reduce the light penetration and aquatic photosynthesis [6]. On the other hand, the pharmaceutical industry widely uses antibiotics, and these activities result in the pharmaceutical ingredients being discharged into the water bodies. These contaminants lead to antibiotic-resistant bacteria and long-term accumulation of harmful substances in ecosystems [7,8].

To overcome this issue, researchers are widely used in different wastewater treatment techniques such as adsorption, coagulation-flocculation, chemical oxidation, and activated sludge processes. These processes have some limitations in industrial effluents [9,10]. In general, textile dyes are highly stable and resistant to biodegradation, so it's highly complicated to remove biological processes [11]. On the other hand, the adsorption process only converts the pollutants from one phase to another phase, and it also creates secondary waste. So, it requires safe disposal of this secondary waste, or further treatment is required [12]. So, these approaches struggle to eliminate hazardous

* Corresponding authors.
E-mail addresses: bhuviphy11@gmail.com (B. Kandasamy), palanisamyg@yu.ac.kr (G. Palanisamy).

https://doi.org/10.1016/j.inoche.2026.116968
Received 20 February 2026; Received in revised form 21 May 2026; Accepted 31 May 2026
Available online 1 June 2026
1387-7003/© 2026 Elsevier B.V. All rights are reserved, including those for text and data mining, AI training, and similar technologies.

pollutants.

Among these approaches, Advanced oxidation processes of photocatalysis are effective treatment techniques due to the low operational cost, minimal secondary pollution, and easy degradation of the hazardous pollutants under light conditions [13–15]. Recently, Transition metal oxides have been gaining attention as photocatalysts due to their effective photocatalytic performance under visible and natural sunlight [16,17]. On the other hand, one of the main challenges in photocatalysis is the low efficacy of solar energy conversion, with approximately 95% of the solar energy being unused. Many traditional photocatalysts can only absorb a small portion of the light in the UV range [18–21]. Also, some oxides can absorb visible light, such as Fe_2O_3 [22], $CoFe_2O_4$ [23] and etc., Compared to the metal oxide, metal sulfides show excellent electronic conductivity, and this behavior making favorable for wastewater treatment [24,25]. Among various metal sulfides, Bi_2S_3 nanoparticles are an efficient photocatalyst for eliminating hazardous pollutants compared to bismuth oxide due to their improved charge carrier generation [26]. Bi_2S_3 has a narrow bandgap (1.3–1.7 eV) and strong visible light absorption; this behavior makes it significant for photocatalytic applications [27]. Under visible light, the performance is low due to the photo corrosion and rapid recombination of charge carriers; these behaviors limit the overall photocatalytic activity [28]. To solve this problem, modify or tune the photocatalyst with other two-dimensional materials to improve their performance under solar light.

Among various 2D materials, the metal-free structure of graphitic carbon nitride (g-C_3N_4) has attracted photocatalyst due to its suitable energy bandgap (~2.7 eV), effective chemical and thermal stability [29]. When combined with Bi_2S_3, a narrow bandgap chalcogenide shows a durable visible light absorption, the Bi_2S_3:g-C_3N_4 heterostructure making more benefits from effective visible light absorption, strong redox potential, efficient charge separation, etc., The metal-free, earth-abundant, and stable materials of g-C_3N_4 added with Bi_2S_3 construct a synergistic effect that expressively enhances photocatalytic performance. However, the detailed mechanism and charge transfer behavior at Bi_2S_3:g-C_3N_4 nanocomposite are still lacking. So, a better understanding of these mechanisms is necessary for improving their photocatalytic efficiency.

In this work, we prepared a Bi_2S_3:g-C_3N_4 heterostructure and used these materials to degrade both dye and pharmaceutical waste. In addition, this work systematically investigates the effect of composite concentrations on photocatalytic efficacy. Furthermore, the various photochemical characterization with recycle test and scavenger experiment to reveal the degradation mechanism and materials reusability. Moreover, the expected integration of g-C_3N_4 with Bi_2S_3 forms a synergistic heterojunction that enhances charge separation, extends light absorption into the visible region, and improves redox capability, overcoming the individual limitations of both components.

2. Materials and methods

Melamine [$C_3H_6N_6$], Bismuth nitrate hexahydrate [Bi $(NO_3)_3.6H_2O$], Methylene blue [$C_{16}H_{18}ClN_3S$], Sodium sulfide [Na_2S], Ethanol [C_2H_5OH], 1, 4-Benzoquinone [$C_6H_4O_2$], Isopropanol [$(CH_3)_2CHOH$], Ciprofloxacin ($C_{17}H_{18}FN_3O_3$), Triethanolamine [$C_6H_{15}NO_3$] and all other chemicals were obtained from Sigma- Aldrich in India.

2.1. Preparation of Bi_2S_3 nanoparticles

The Bi_2S_3 nanoparticles were prepared using a hydrothermal approach with a Bi source as the precursor. One mole of $Bi(NO_3)_3$ was dissolved in 50 mL of DDW, and 30 mL of Na_2S solution (1 mol) was slowly added to the above solution under continuous stirring. Then, the whole solution was transferred into an autoclave. The reaction temperature was then maintained at 160 °C for 12 h in a hot air oven. The obtained mixed solution was washed with DDW and centrifuged several times. The obtained powder was dried at 60 °C for 12 h.

2.2. Preparation of g-C_3N_4

The thermal pyrolysis technique was used to produce the g-C_3N_4 [30]. The melamine is heated at 550 °C for 3 h. at a step of 10 °C per 5 min under an air atmosphere. After the furnace was allowed to cool to room temperature, the yellow color samples were ground into a fine powder.

The thermal pyrolysis of the conversion of melamine to g-C_3N_4 can be denoted as follows:

$$6C_3H_6N_6\ (\text{at } 550^{\circ}\text{C}) \rightarrow 7(C_3N_4) + 3NH_3$$

2.3. Preparation of Bi_2S_3:g-C_3N_4 nanocomposites

The Bi_2S_3:g-C_3N_4 nanocomposite was prepared following a similar procedure to that used for bare Bi_2S_3, with the addition of 0.5 g of gC_3N_4. All hydrothermal reaction conditions, including molar ratio, reaction time and temperature were maintained the same. In details, after the S^{2-} ions solution was added to the existence of the g-C_3N_4 and Bi precursor solution. This hydrothermal process makes uniform evolution of Bi_2S_3 nanoparticles on the g-C_3N_4 surface, confirming strong interfacial bonding and efficient heterojunction formation. A similar process was repeated to prepare different weight ratios (1:0.5, 1:1, and 0.5:1) of Bi_2S_3:g-C_3N_4 nanocomposite.

2.4. Photocatalytic activity analysis of as-prepared samples

The photocatalytic performance of the prepared photocatalysts was evaluated using MB and CPF as model pollutants. For each experiment, 10 mg of the photocatalyst was dispersed in 50 mL of an aqueous dye solution with an initial concentration of 10 ppm. The reaction mixture was then subjected to visible light irradiation to activate the photocatalytic process. 2 mL of the treated solution was taken, and the UV absorption spectra were tested to monitor the degradation progress. The MB (664 nm) and CPF (~350 nm) dye concentrations were analyzed using a UV–Visible spectrophotometer. A scavenger study was used to determine which reactive species play a major role in the degradation process. Various scavengers such as IPA, BQ, TEOA were used to determine hydroxyl radicals ($^{\bullet}OH$), superoxide radicals ($^{\bullet}O_2^-$), electrons, and photogenerated holes (h^+) scavenger, respectively. This scavenger test provided the photocatalytic mechanism of the degradation process. The cyclic stability of the g-C_3N_4/Bi_2S_3 photocatalyst was assessed over five cycles. After every cycle, the photocatalyst was recovered by centrifugation and washed multiple times with DDW. The obtained photocatalyst was dried overnight before being reused in the next cycle. This method confirmed that the photocatalysts' performance and stability were constantly checked during the constant investigations.

The degradation efficacy of the prepared materials was evaluated by utilizing Eq. (1):

$$\text{Removal efficiency} = \left(\frac{C_0 - C_i}{C_0}\right) \times 100 \quad (1)$$

where C_0 (mg/L) and C_i (mg/L) are the determined initial and final concentrations of dyes.

The rate constants were analyzed using the pseudo-first-order kinetic Eq. (2) [31]:

$$\frac{(\ln (C_i))}{C_0} = -k_1 t \quad (2)$$

where C_0 (mg/L) and C_i (mg/L) are the measured initial and time concentrations of dyes, respectively, and t is the time interval.

2.5. Characterization

The phase purity and structure of the prepared samples were

revealed via X-ray diffraction (XRD) analysis, and this analysis was studied using a Philips X'Pert diffractometer (Cu Kα radiation-λ = 1.54046 Å). Fourier-transform infrared (FTIR) spectroscopy was employed to study the functional groups present in the prepared samples. The FTIR spectra were acquired using a Bruker Alpha-E spectrophotometer, scanning the wavenumber range of 4000 to 400 cm^{-1}. The morphological features, selected area electron diffraction (SAED) patterns, and interplanar spacing of the hybrid sample were examined using a JEOL JED 2300 high-resolution transmission electron microscopy (HR-TEM), supplemented with EDS capabilities. X-ray Photoelectron spectroscopy (XPS) analysis was performed by a PHI Versaprobe III (ULVAC PHI) instrument. Hence, the Ultraviolet–Visible diffuse reflectance spectroscopy (UV–Vis DRS) analysis was performed to observe the optical absorption properties and energy band gap of the prepared samples.

3. Results and discussion

Fig. 1(a–c) presents HRTEM images of the (0.5:1) g-C_3N_4:Bi_2S_3 hybrid nanoparticles, providing insights into their intricate morphology. The images reveal distinct sheet- and rod-like structures, as shown in Fig. 1(a) and (b), which correspond to the g-C_3N_4 and Bi_2S_3 nanoparticles, respectively. The g-C_3N_4 nanoparticles show the irregular 2D sheet-like structures (wrinkle-like texture) with particle sizes ranging from 50 to 200 nm, respectively [32]. This sheet-like morphology is very helpful for photocatalytic applications [33].

The g-C_3N_4 nanosheets combine with Bi_2S_3 nanorods to exhibit a synergistic effect, and these behaviors develop an efficient dye degradation property. In Fig. 1(c), the Bi_2S_3:g-C_3N_4 hybrid nanosheets show the crystalline nature of the nanoparticles and the lattice spacings of 0.23 nm and 0.35 nm, corresponding to the (1 4 1) and (1 1 1) planes of Bi_2S_3 and g-C_3N_4, respectively. In Fig. 1(d), Bi_2S_3:g-C_3N_4 hybrid nanosheets of selected area electron diffraction (SAED) patterns exhibit a combination of diffraction dots and diffraction rings. Diffraction dots of Bi_2S_3 are interspersed with diffraction rings of g-C_3N_4. Based on this morphology and SAED pattern, the results clearly show the hybrid formation of Bi_2S_3 and g-C_3N_4 nanoparticles. These combined synergistic effects may be helpful for the photocatalytic degradation of hazardous pollutants. [26,34]

The XRD patterns of pure Bi_2S_3 and g-C_3N_4 and the different weight ratios of the hybrid materials are shown in Fig. 1(e). The XRD pattern of Bi_2S_3 (Pnma space group) displayed diffraction peaks at 2θ values of 24.9°, 28.65°, 31.86°, 32.87°, 34.27°, 39.84°, 45.62°, 46.72°, 52.81°, 54.64°, 59.12°, 62.47°, 65.17°, 67.91°, and 69.46° correspond to the (0 1 3), (0 2 3), (1 2 2), (1 3 0), (0 3 3), (1 1 4), (2 0 0), (1 5 0), (2 3 1), (0 3 6), (2 2 4), (0 3 7), (1 7 2), (0 8 1), and (1 6 5) planes, respectively. These peaks are well matched to the orthorhombic phase of Bi_2S_3 (JCPDS:65-3884).

The g-C_3N_4 diffraction pattern shows the two characteristic peaks at 12.9° (d = 0.67 nm) and 27.52° (d = 0.336 nm), ascribed to the (1 0 0) and (0 0 2) lattice planes, respectively. The corresponding diffraction planes are well matched with the hexagonal phase of g-C_3N_4 (JCPDS:87-1526). The (0 0 2) peak is a typical interlayer stacking reflection, indicative of the conjugated aromatic arrangements observed in bulk g-C_3N_4. These results confirm the formation of graphitic carbon nitride in the synthesized samples. The diffraction patterns of Bi_2S_3:g-C_3N_4 at weight ratios of 1:0.5, 1:1, and 0.5:1 exhibit strong agreement with the characteristic peaks of Bi_2S_3 and g-C_3N_4 nanoparticles, confirming the successful formation of the Bi_2S_3:g-C_3N_4 hybrid structure.

Fig. 1(f) shows the FTIR spectrum of the as-prepared samples, which was used to identify the presence of functional groups in the prepared samples. Across the entire spectrum, the bands observed between 3200 and 3600 cm^{-1} correspond to the O-H bond vibration of surface-adsorbed water molecules. The peaks at 615 and 532 cm^{-1} can be assigned to Bi-S bonding links [35]. Similarly, the presence of a vibrational band at 1110 cm^{-1} characterizes the S-H asymmetric bond of Bi_2S_3 [27]. For the pure g-C_3N_4, the firm peaks observed at approximately 1237, 1318, 1404, and 1464 cm^{-1} correspond to the aromatic C-N stretching vibrations. Likewise, the C═N stretching vibrations were observed from the peaks that appeared at 1636 cm^{-1} [36]. The FTIR spectra of the as-prepared nanocomposites show only g-C_3N_4 and Bi_2S_3 functional groups, and a slight shift in band positions occurred at higher g-C_3N_4 content. This shift may be attributed to the combined hybrid formation with g-C_3N_4 and Bi_2S_3.

The effectiveness of photocatalysts in their ability to catalyze chemical reactions using light is influenced by several factors. These include the efficiency of generating, separating, and transporting the photogenerated carriers, which are dependent on the light absorption band edge, band gap energy, and the fate of electron-hole pairs. The observed UV-DRS spectra of the prepared samples are shown in Fig. 2. The UV-DRS absorption of Bi_2S_3 is comparatively lower than that of all other as-prepared samples. Similarly, when compared to the Bi_2S_3 nanoparticles, the g-C_3N_4 nanosheets show a high absorption profile in the entire UV and visible light region. Surprisingly, after the addition of

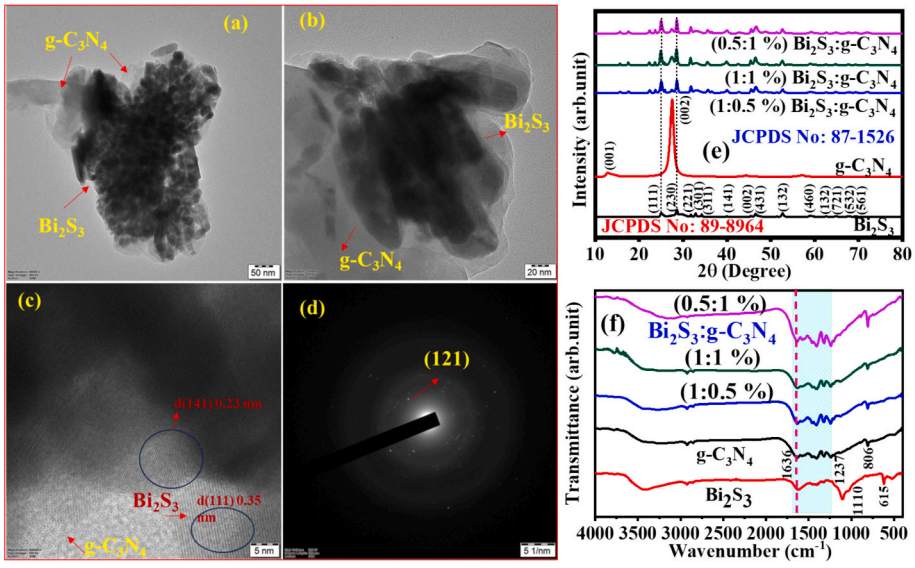


Fig. 1. (a–c) HRTEM images and (d) SAED patterns of (0.5:1%) Bi_2S_3:g-C_3N_4 (e) XRD pattern and (f) FTIR spectra of as-prepared samples.

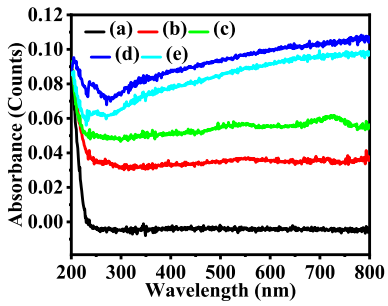


Fig. 2. UV-DRS spectra for (a) Bi_2S_3, (b) g-C_3N_4, (c) (1:0.5%) Bi_2S_3:g-C_3N_4 (d) (1:1%) Bi_2S_3:g-C_3N_4 (c) (0.5:1%) Bi_2S_3:g-C_3N_4.

g-C_3N_4 with Bi_2S_3 in different wt% ratios, the absorption enhancement was observed in the entire spectra. The observed enhancement was owed to the synergistic effect between the Bi_2S_3 and g-C_3N_4 nanomaterials. In particular, the (1:1%) Bi_2S_3:g-C_3N_4 samples show enhanced absorption in the entire spectrum. As observed from the UV-DRS results, the (1:1%) Bi_2S_3:g-C_3N_4 samples can be used as an effective photocatalyst under UV–visible light irradiation for the removal of toxic pollutants.

Bi_2S_3 is a narrow bandgap material (1.3 eV) [37], and it is active for visible light. Similarly, g-C_3N_4 is an organic material (~2.7 eV) [38], and it is active for UV light. When these two materials are combined in a (0.5:1%) ratio, the enhanced absorption in the whole spectrum. This is due to the efficient separation of photo-induced electron-hole pairs and helps charge transfer between the two materials. UV-DRS results of 0.5:1% Bi_2S_3:g-C_3N_4 samples have a high absorption behavior for UV–Visible light (Fig. 2). This improved absorption performance is important for photocatalytic treatments because this material absorbs a wide range of wavelengths and generates many electron-hole pairs.

Fig. 3 shows the survey spectra of the Bi_2S_3:g-C_3N_4 (0.5:1%) hybrid sample, suggesting the presence of Bi, S, O, C, and N. The high-resolution Bi 4f spectrum was deconvoluted into two major binding energy peaks, corresponding to $4f_{7/2}$ and $4f_{5/2}$, observed at 158.7 eV and 163.7 eV, respectively, which are commonly associated with Bi-S bonding of Bi_2S_3 [39,40]. It can therefore be concluded that bismuth predominantly exists in the +3-oxidation state. Additionally, certain peaks observed at corresponding binding energy values align with the +2 oxidation state, providing strong evidence for the formation of Bi^{2+} defective sites in the synthesized photocatalyst [41]. The S 2s spectrum exhibits a peak at 227.3 eV corresponding to the Bi-S interfaces [42–44]. The O 1 s spectrum exhibits a signal at 532.5 eV, which can be attributed to either the irreversibly adsorbed molecular mode or C-O interactions [42,43]. The C 1s spectra were deconvoluted into two peaks at 284.5 eV and 286.9 eV, corresponding to adventitious carbon (C-C) and N-C=N bonds, respectively. In the C 1s spectrum of the Bi_2S_3:g-C_3N_4 hybrid sample, the N-C=N peak exhibited a shift of 0.5 eV towards higher binding energy, which may be attributed to the strong interfacial interaction within the prepared sample [42]. In Fig. 3, the N 1S spectra show four deconvolution peaks at 397.8, 398.9, 400.3, and 402.3 6 eV. The major signals observed at 397.8 and 398.9 eV are attributed to N(C_2) and (N($C)_3$), respectively [45,46]. Similarly, the binding energies at 400.3 and 402.3 eV are related to the tertiary N atoms ((C-N(H)-C or C-N(-C)-C)) and charging impacts, respectively [47]. The XPS spectra of Bi_2S_3:g-C_3N_4 hybrid nanoparticles exhibit distinct features, reflecting their unique contributions to the hybrid material.

The energy band gap, band edge positions, effective mass, and absorption edges were obtained from the "The materials project" (*Data retrieved)* files to confirm the theoretical conformation(Fig. 4) of electronic state and DOS, and their observed results were shown in Table 1 [48,49]. The band gaps of Bi_2S_3 (1.8 eV) and g-C_3N_4 (2.2 eV) obtained from the DOS indicate strong visible-light absorption, making them promising for photocatalysis. Their valence and conduction band positions support efficient redox reactions, facilitating water splitting. Favorable charge transport properties, including high carrier mobility and reduced recombination, enhance photocatalytic efficiency. A high density of states near the band edges improves charge carrier availability. Optical absorption edges at 885 nm (Bi_2S_3) and 564 nm (g-C_3N_4) confirm their visible-light activity. These properties highlight their

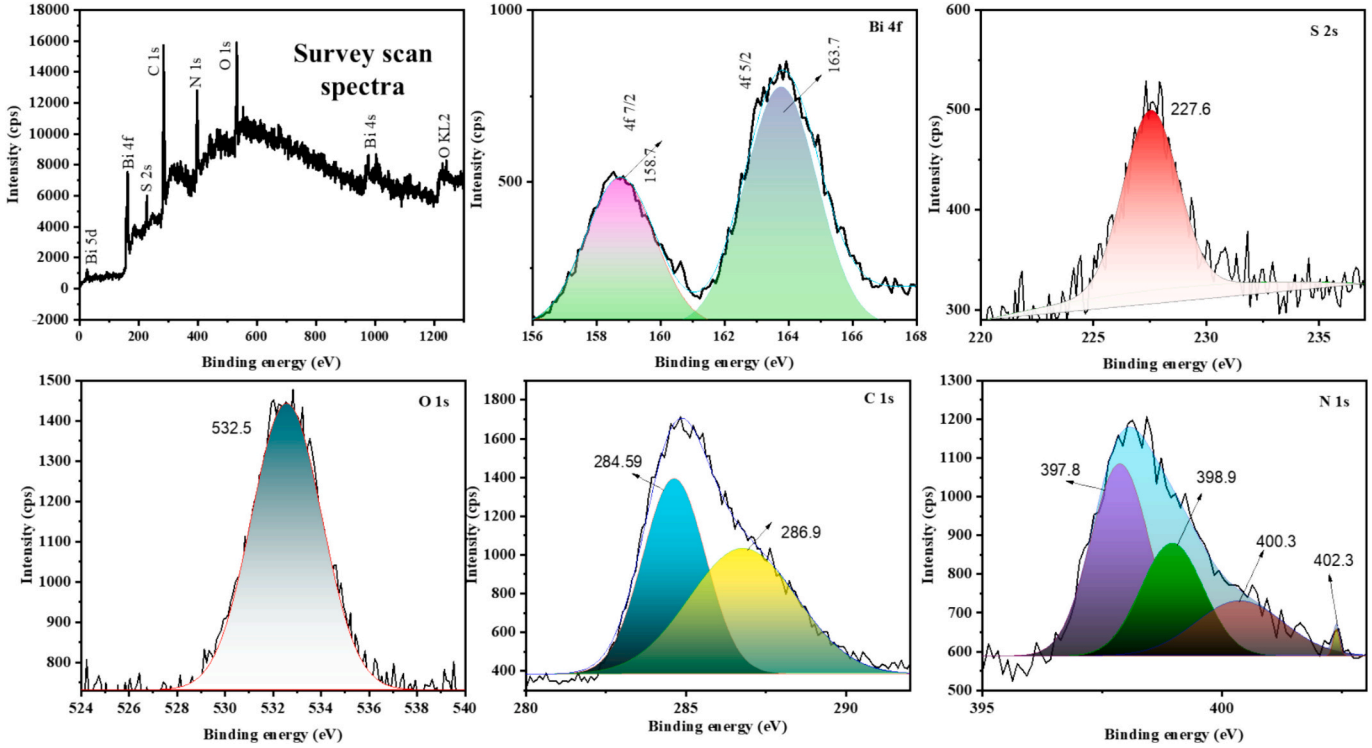


Fig. 3. XPS spectra of Bi_2S_3:g-C_3N_4 (0.5:1%) hybrid nanoparticles.

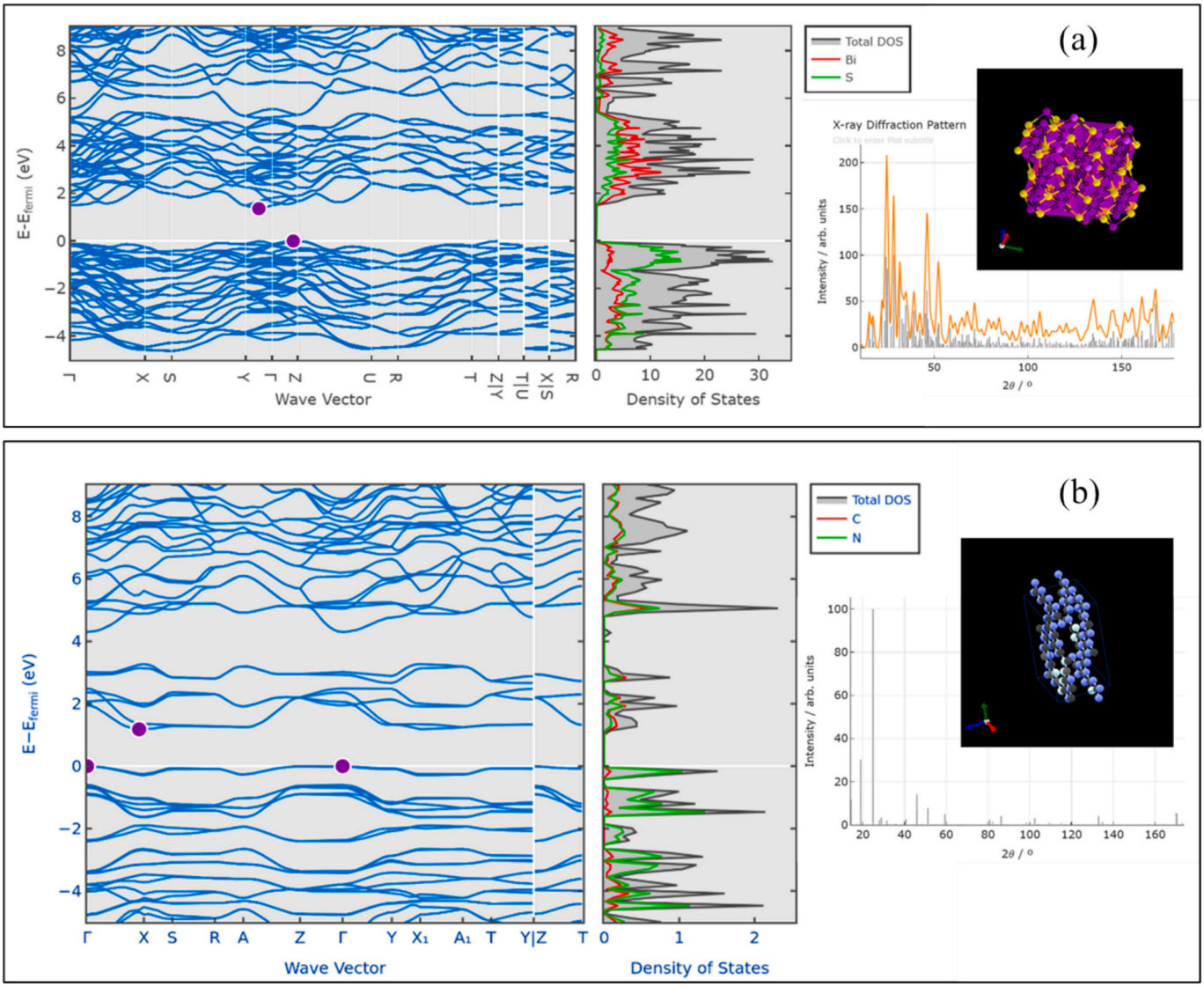


Fig. 4. Electronic state of Bi_2S_3 and g-C_3N_4 obtained from "The Materials Project".

Table 1
Comparison of the electronic and optical properties of Bi_2S_3 and g-C_3N_4.

Property	Bi_2S_3	g-C_3N_4
Bandgap (Eg) (eV)	1.8 (theroatical value)	2.2 (theroatical value)
VBM Position (eV vs. NHE)	0 eV	+1.4
CBM Position (eV vs. NHE)	~1. 8	−0.8
Charge Carrier Mobility (μe, μh)	180 cm^2/Vs (e^-) and 120 cm^2/Vs(h^+)	120 cm^2/Vs (e^-), 80 cm^2/Vs (h^+)
Effective Mass (m*)	0.29 m_e (e^-), and 0.35 m_e (h^+)	0.4 m_e (e^-), and 0.6 m_e (h^+)
Absorption Edge (λ)	885 nm	~562

potential for solar-driven photocatalytic applications.

Photocatalytic degradation of MB and CPF

The photocatalytic degradation ability of the as-prepared samples was examined with the help of a 500 W xenon lamp as the visible light source, against the MB dye. Fig. 5(a) shows the degradation of MB over (0.5:1%) Bi_2S_3:g-C_3N_4 of as-prepared samples with different irradiation time intervals. The ad/desorption capability of the as-prepared samples was studied under dark conditions for 60 min, and it doesn't have noticeable adsorption behavior over the period of time. In Fig. 5(b), within 75 min of irradiation, the efficiencies for degradation of MB dye by g-C_3N_4, Bi_2S_3, (1:0.5%) Bi_2S_3:g-C_3N_4, (1:1%) Bi_2S_3:g-C_3N_4, and (0.5:1%) Bi_2S_3:g-C_3N_4 were 45.4, 58.5, 76.0, 78, and 98.4%, respectively. Compared with the pure Bi_2S_3, g-C_3N_4, and other hybrid samples, the (0.5:1%) Bi_2S_3:g-C_3N_4 hybrid nanomaterial has high photocatalytic activities, which indicates that the Bi_2S_3:g-C_3N_4 nanocomposites produced by interfacial connection played key roles.

The degradation activity of the prepared samples is compared in Fig. 5(c), which plots the changes in MB concentration at 664 nm as a function of irradiation time. The observed results clearly demonstrate that the hybrid samples possess enhanced catalytic activity relative to the pristine samples. The reaction kinetics of the photodegradation process were investigated using a pseudo-first-order kinetic equation model, and the corresponding kinetic plot is presented in Fig. 5(d). The calculated correlation coefficient values were 0.989, 0.989, 0.951, 0.990, and 0.933 for the g-C_3N_4, Bi_2S_3, (1:0.5%) Bi_2S_3:g-C_3N_4, (1:1%) Bi_2S_3:g-C_3N_4, and (0.5:1%) Bi_2S_3:g-C_3N_4. The relatively lower R^2 value of 0.933 for (0.5:1%) Bi_2S_3:g-C_3N_4 nanocomposite, despite its high photocatalytic efficiency, could be attributed to several factors like complex reaction kinetics, charge carrier dynamics, surface saturation

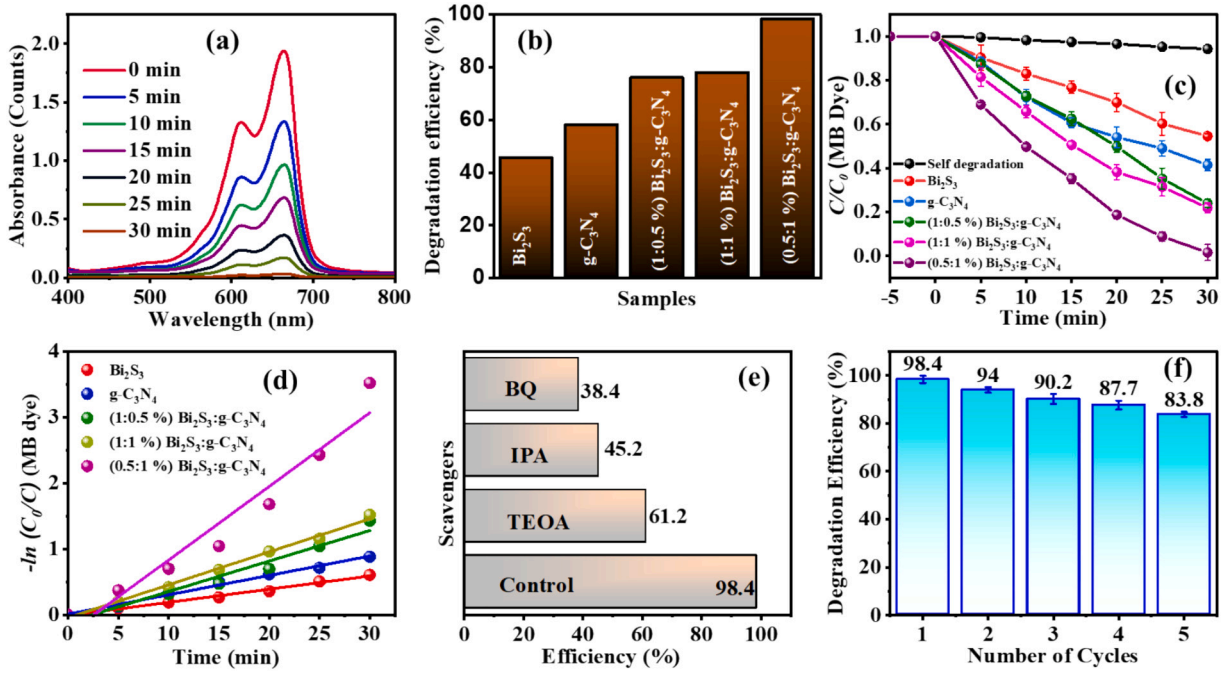


Fig. 5. (a) UV–Visible absorption spectra of MB dye in (0.5:1%) Bi_2S_3:g-C_3N_4 nanocomposite, (b) photocatalytic degradation efficiency of prepared sample, (c) C/C_0 vs. irradiation time curves, (d) Natural logarithm C_0/C fitting curves, (e) radical trapping analysis (0.5:1%) Bi_2S_3:g-C_3N_4 nanocomposite over different scavengers, and (f) cyclic analysis of (0.5:1%) Bi_2S_3:g-C_3N_4 nanocomposite.

effect, etc. [50,51].

The fundamental mechanisms underlying the photodegradation process in Bi_2S_3:g-C_3N_4 nanocomposites were investigated using radical trapping analysis (RTA). Fig. 5(e) illustrates the outcomes obtained from various radical trapping experiments conducted to assess the effects on MB dye degradation under UV–Visible irradiation. The RTA was performed in the presence of h^+, superoxide, and OH^- scavengers, such as TEOA, BQ, and IPA. From the observed result, it was observed that the superoxides and OH* led to a significant inhibition of the MB degradation reaction, with a degradation efficiency of 38.4% and 45.2%, respectively. Furthermore, the addition of TEOA acting as a trapping agent for the hole resulted in the inhibition of approximately 61.2% of the degradation process. Based on these results, superoxide radicals (O_2^-) play a main role in the degradation of the MB dye within the Bi_2S_3: g-

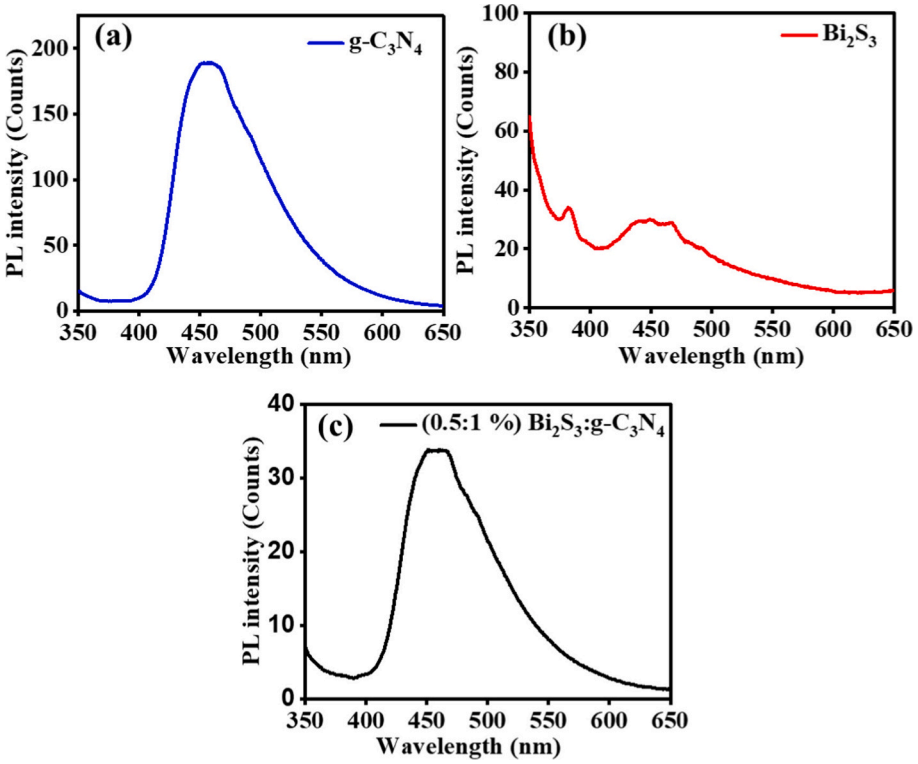


Fig. 6. PL analysis of (a) gC_3N_4 (b) Bi_2S_3 and (c) (0.5:1%) Bi_2S_3:g-C_3N_4 nanocomposite.

C_3N_4 nanocomposites.

Recycle tests are very important from a practical application point of view. This study's focus is to reuse and recover the catalyst multiple cycles without loss of activity. (0.5:1%) Bi_2S_3: g-C_3N_4 nanocomposite catalyst was tested in five successive cycles to study its photocatalytic cyclic performance (Fig. 5(f)). In each photocatalytic cycle, the hybrid nanoparticles were separated from the dye solution and washed with DDW to finally dry overnight. The results clearly show that 83.8% degradation of MB dye in the catalyst's performance after five consecutive cycles. The FTIR spectra (Fig. S1) showed that the corresponding functional groups and vibrational bands of Bi_2S_3 and g-C_3N_4 ascribed after the 5th cycle reaction. No significant major changes were observed.

The PL Spectra of the bare gC_3N_4, Bi_2S_3 and (0.5:1%) Bi_2S_3:g-C_3N_4 nanocomposite were studied and the corresponding results are shown in Fig. 6. The PL spectra of these samples were anlayzed in the wavelength range of 350–650 nm using an excitation wavelength of 340 nm. The bare g-C_3N_4 samples exhibits a strong and broad emission intensity at around 454 nm, indicating excitonic band to band irradiative emission [52]. After the combine of Bi_2S_3 with g-C_3N_4, the composite showed a significantly decreased PL intensity. This reduction may be due to the recombination of charge carriers was effectively suppressed after the composite formation. This lower emission intensity indicates the improved migration and separation of e^--h^+ pair [53]. Based on these results, the (0.5:1%) Bi_2S_3:g-C_3N_4 nanocomposite shows improved charge transfer behavior, leading to improved the photocatlatyic dye degradation performance.

On the other hand, the large use of antibiotics in medical treatment has caused serious environmental pollution [54]. After treatment, these antibiotics are not fully metabolized in humans and animals, and this maximum amount is discharged into the ecosystem. Ciprofloxacin (CPF), a highly effective and wide-spectrum antibiotic, is one of the major contributors to this problem. In recent years, photocatalysis has been a promising green technology for the effective removal of antibiotics, including CPF, from water systems [55]. Fig. 7(a) displays the photocatalytic degradation performance of CPF using the as-prepared (0.5:1%) Bi_2S_3:g-C_3N_4 nanocomposite. The photocatalytic degradation experiment was carried out for 60 min under UV–visible light irradiation. The samples were collected and analyzed at 15-min intervals to evaluate photocatalytic performance. Fig. 7(b) shows the bar diagram of time vs degradation efficiency clearly shows the (0.5:1%) Bi_2S_3:g-C_3N_4 nanocomposite shows the 84.28% CPF degradation within 60 min. Fig. 7 (c) shows the change in dye concentration(C/C_0) of CPF vs time. The results clearly indicate that the maximum absorption intensity of CPF concentration significantly decreased. The observed degradation kinetics followed pseudo first order kinetics (Fig. 7(d)), suggesting that the (0.5:1%) Bi_2S_3:g-C_3N_4 nanocomposite facilitates efficient charge carrier separation, transfer, and utilization, ultimately leading to enhanced photocatalytic degradation of CPF.

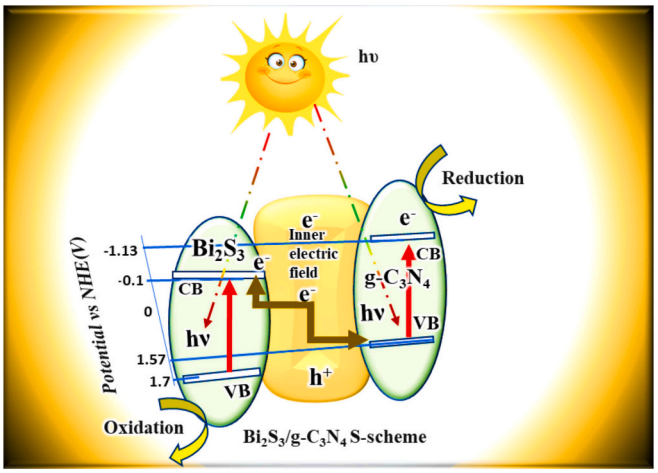


Fig. 8. Photocatalytic degradation mechanism of as (0.5:1%) Bi_2S_3:g-C_3N_4 nanocomposite.

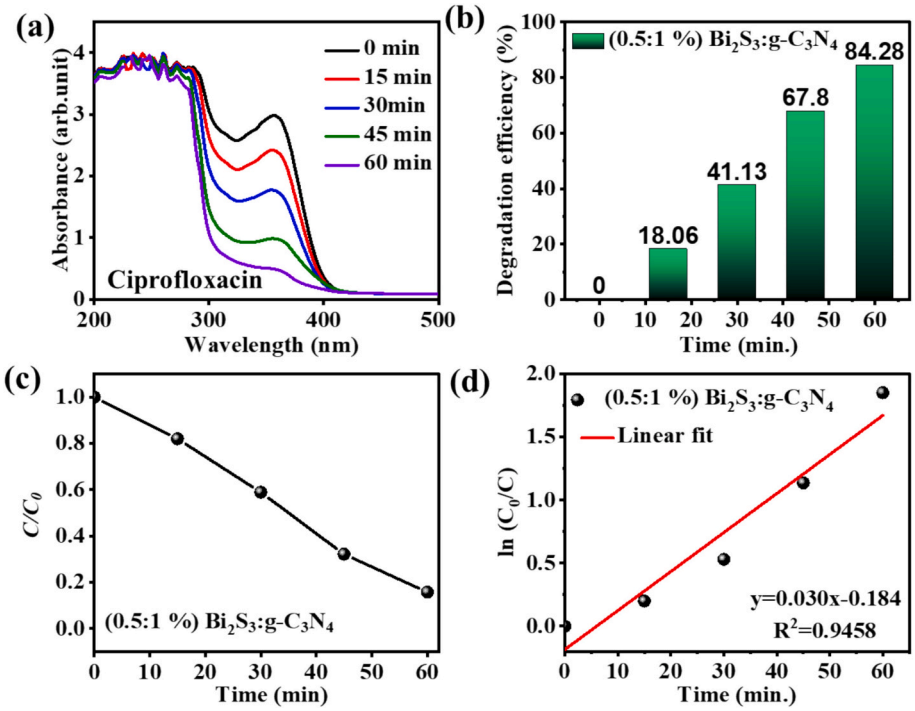


Fig. 7. (a) Photocatalytic degradation of CPF (b) degradation efficiency at different time, (c) C/C_0 versus irradiation time and pseudo first kinetic plot of the as-prepared (0.5:1%) Bi_2S_3:g-C_3N_4 hybrid photocatalyst.

Reaction mechanism

The photocatalytic mechanism of the (0.5:1%) Bi_2S_3:g-C_3N_4 nanocomposite is shown in Fig. 8. As shown in Fig. 8, when exposed to visible light, electrons in the valence band (VB) of both Bi_2S_3 and g-C_3N_4 are excited and transition to the conduction band (CB), creating electron-hole (e^-/h^+) pairs. When the two materials in close contact, formidable internal electric field (IEF) and bending of the energy band edges is formed at their interface [56]. Due to the energy band positions of Bi_2S_3 and g-C_3N_4, are promotes the incident light absorption and help the generation of more charge carriers [57,58]. In the S- scheme system, the electrons in the CB of Bi_2S_3 recombine with the holes in the valence band of g-C_3N_4 at the inferface. This process leave the electrons in the CB of g-C_3N_4 and the holes in the VB of Bi_2S_3, both of which have stronger redox ability. As a results, the photocatalyst can more effectively drive surface reactions during MB degradation.

The remaining electrons on g-C_3N_4 react with dissolved oxygen to produce superoxide radicals (O_2*). The generated superoxide radicals can subsequently participate in the degradation of organic pollutants, highlighting the significance of this reaction in the photocatalytic process. Superoxide radicals can further react with H_2O to produce hydroxyl radicals (•OH), which play an important role in the oxidation and degradation of MB dye. The formation of superoxide radicals helps the photo generated electrons produced during photoexcitation, thereby reducing the electron-hole recombination.

At the same time, the VB edge of Bi_2S_3 (+1.7 eV) is more positive than that of the VB edge of g-C_3N_4 (+1.57 eV), which allows the hole transfer from Bi_2S_3 to g-C_3N_4. The holes remaining in the VB of Bi_2S_3 can react with H_2O to produce hydroxyl radicals (•OH) as shown in reaction (1). These hydroxyl radicals are highly reactive species that effectively degrade the MB dye.

$$h^+ (VB) + H_2O \rightarrow {}^{\cdot}OH + H^+ \quad (1)$$

In addition, the internal electric field at the heterojunction interface promotes efficient charge carrier separation. More charge carriers are available to participate in the photocatalytic reaction, to improve the photocatalytic performance of MB dye.

4. Conclusion

Effective treatment of wastewater is necessary for maintaining human health, defending aquatic ecosystems, and ensuring the sustainable use of water resources. Therefore, it is important to develop advanced treatment technologies and support environmentally friendly approaches to reduce water pollution. In this study, the removal of MB and CPF was tested using a (0.5:1%) Bi_2S_3:g-C_3N_4 1D/2D hybrid photocatalyst. Detailed characterization of the prepared material was carried out using XRD, HRTEM, UV, XPS, and FTIR techniques to understand its structural, morphological, and photophysical properties. In addition, UV–Vis DRS analysis was used to explore its optical absorption properties.

When compared with pure Bi_2S_3 and g-C_3N_4, the Bi_2S_3:g-C_3N_4 (0.5:1) hybrid photocatalyst exhibited better photocatalytic performance (98.4%- MB and 84.28%-CPF). This higher activity can be attributed to improved electron-hole separation, many active surface sites, and more efficient charge transfer. These properties can be extensively supported by the effective degradation of hazardous pollutants. Superoxide and hydroxyl radicals play a major role in the degradation performance of MB and CPF. Overall, this study presents a useful way to develop a sustainable water treatment approach. Future work should focus on further optimization and practical application of this photocatalyst to expand its potential in large-scale water treatment systems.

CRediT authorship contribution statement

Bhuvaneswari Kandasamy: Writing – review & editing, Writing – original draft, Supervision, Project administration, Methodology, Conceptualization. **Balaji Parasuraman:** Visualization, Formal analysis, Data curation. **Pugazhenthiran Nalenthiran:** Writing – review & editing, Methodology. **S. Manimegalai:** Visualization, Validation, Data curation. **Sivaprakash Paramasivam:** Validation, Methodology, Data curation. **Pazhanivel Thangavelu:** Validation, Investigation, Data curation. **Ikhyun Kim:** Validation, Data curation. **Jintae Lee:** Visualization, Validation, Data curation. **Govindasamy Palanisamy:** Writing – review & editing, Writing – original draft, Methodology, Investigation.

Declaration of competing interest

The authors declare that they have no known competing financial interests or personal relationships that could have appeared to influence the work reported in this paper.

Appendix A. Supplementary data

Supplementary data to this article can be found online at https://doi.org/10.1016/j.inoche.2026.116968.

Data availability

Data will be made available on request.

References

[1] S. Afzal, M.N. Akhtar, L. Gurbanova, M.A. El-Sheikh, A. Ahmad, C.H. Choi, M. R. Karim, S.S.A. Shah, M.A. Nazir, Synergistic effect SnO_2/g-C_3N_4 heterojunction cocatalyst for photodegradation of methyl orange, ChemistrySelect 10 (2025), https://doi.org/10.1002/slct.202502037.
[2] M.I. Din, A.G. Nabi, Z. Hussain, M. Arshad, A. Intisar, A. Sharif, E. Ahmed, H. A. Mehmood, M.L. Mirza, Innovative seizure of metal/metal oxide nanoparticles in water purification: a critical review of potential risks, Crit. Rev. Anal. Chem. 49 (2019) 534–541, https://doi.org/10.1080/10408347.2018.1564647.
[3] X. Zhang, M.Z. Yates, Enhanced photocatalytic activity of TiO_2 nanoparticles supported on electrically polarized hydroxyapatite, ACS Appl. Mater. Interfaces 10 (2018) 17232–17239, https://doi.org/10.1021/acsami.8b03838.
[4] C. Gao, W. Yu, Y. Zhu, M. Wang, Z. Tang, L. Du, M. Hu, L. Fang, X. Xiao, Preparation of porous silicate supported micro-nano zero-valent iron from copper slag and used as persulfate activator for removing organic contaminants, Sci. Total Environ. 754 (2021), https://doi.org/10.1016/j.scitotenv.2020.142131.
[5] W. Hou, S.B. Cronin, A review of surface plasmon resonance-enhanced photocatalysis, Adv. Funct. Mater. 23 (2013) 1612–1619, https://doi.org/10.1002/adfm.201202148.
[6] M.Y. Guo, A.M.C. Ng, F. Liu, A.B. Djurišić, W.K. Chan, Photocatalytic activity of metal oxides-the role of holes and $OH^{\cdot}$ radicals, Appl. Catal. Environ. 107 (2011) 150–157, https://doi.org/10.1016/j.apcatb.2011.07.008.
[7] S. Panneri, P. Ganguly, M. Mohan, B.N. Nair, A.A.P. Mohamed, K.G. Warrier, U. S. Hareesh, Photoregenerable, bifunctional granules of carbon-doped g-C_3N_4 as adsorptive photocatalyst for the efficient removal of tetracycline antibiotic, ACS Sustain. Chem. Eng. 5 (2017) 1610–1618, https://doi.org/10.1021/acssuschemeng.6b02383.
[8] G. Salehi, R. Abazari, A.R. Mahjoub, Visible-light-induced graphitic-C_3N_4@nickel-aluminum layered double hydroxide nanocomposites with enhanced photocatalytic activity for removal of dyes in water, Inorg. Chem. 57 (2018) 8681–8691, https://doi.org/10.1021/acs.inorgchem.8b01636.
[9] M. Adachi-Pagano, C. Forano, J.P. Besse, Delamination of layered double hydroxides by use of surfactants, Chem. Commun. (2000) 91–92, https://doi.org/10.1039/a908251d.
[10] M.H. Habibi, N. Talebian, Photocatalytic degradation of an azo dye X6G in water: a comparative study using nanostructured indium tin oxide and titanium oxide thin films, Dyes Pigments 73 (2007) 186–194, https://doi.org/10.1016/j.dyepig.2005.11.006.
[11] L. Wang, M. Zheng, Z. Xie, Nanoscale metal-organic frameworks for drug delivery: a conventional platform with new promise, J. Mater. Chem. B 6 (2018) 707–717, https://doi.org/10.1039/c7tb02970e.
[12] V. Etacheri, C. Di Valentin, J. Schneider, D. Bahnemann, S.C. Pillai, Visible-light activation of TiO_2 photocatalysts: advances in theory and experiments, J. Photochem. Photobiol. C Photochem. Rev. 25 (2015) 1–29, https://doi.org/10.1016/j.jphotochemrev.2015.08.003.
[13] X. Li, J. Yu, S. Wageh, A.A. Al-Ghamdi, J. Xie, Graphene in photocatalysis: a review, Small 12 (2016) 6640–6696, https://doi.org/10.1002/smll.201600382.

[14] S. Kampouri, K.C. Stylianou, Dual-functional photocatalysis for simultaneous hydrogen production and oxidation of organic substances, ACS Catal. 9 (2019) 4247–4270, https://doi.org/10.1021/acscatal.9b00332.

[15] M. Peng, J. Jiang, Y.H. Wang, T. Li, Z. Yang, H.T. Zhu, W.M. He, Semiheterogeneous intrinsic CoS_2-photoredox/Cp_2Fe dual-catalyzed synthesis of selenylated phenanthrene, J. Org. Chem. 90 (2025) 18255–18261, https://doi.org/10.1021/acs.joc.5c02498.

[16] J. Bedia, V. Muelas-Ramos, M. Peñas-Garzón, A. Gómez-Avilés, J.J. Rodríguez, C. Belver, A review on the synthesis and characterization of metal organic frameworks for photocatalytic water purification, Catalysts 9 (2019), https://doi.org/10.3390/catal9010052.

[17] T. Narkbuakaew, P. Sujaridworakun, Synthesis of tri-S-triazine based g-C_3N_4 photocatalyst for cationic rhodamine B degradation under visible light, Top. Catal. 63 (2020) 1086–1096, https://doi.org/10.1007/s11244-020-01375-z.

[18] P. Argurio, E. Fontananova, R. Molinari, E. Drioli, Photocatalytic membranes in photocatalytic membrane reactors, Processes 6 (2018) 162, https://doi.org/10.3390/pr6090162.

[19] B. Yuan, Z. Chu, G. Li, Z. Jiang, T. Hu, Q. Wang, C. Wang, Water-soluble ribbon-like graphitic carbon nitride (g-C_3N_4): green synthesis, self-assembly and unique optical properties, J. Mater. Chem. C 2 (2014) 8212–8215, https://doi.org/10.1039/c4tc01421a.

[20] R. Asahi, T. Morikawa, T. Ohwaki, K. Aoki, Y. Taga, Visible-light photocatalysis in nitrogen-doped titanium oxides, Science (80-.) 293 (2001) 269–271, https://doi.org/10.1126/science.1061051.

[21] K. Kabra, R. Chaudhary, R.L. Sawhney, Treatment of hazardous organic and inorganic compounds through aqueous-phase photocatalysis: a review, Ind. Eng. Chem. Res. 43 (2004) 7683–7696, https://doi.org/10.1021/ie0498551.

[22] G. Zhang, T. Ge, Y. Zhang, E. Zhang, H. Ma, J. Hou, Hydrothermal preparation of Nb^{5+}-doped α-Fe_2O_3 nanorods for efficient visible light-driven photocatalytic reduction of hexavalent chromium, Powder Technol. 436 (2024) 119480, https://doi.org/10.1016/j.powtec.2024.119480.

[23] G. Zhang, J. Guo, J. Hou, E. Zhang, G. Wang, Y. Zhang, Synergetic enhancement of the photocatalytic activity of magnetic $CoFe_2O_4$ by doping Zn^{2+} and combining with conjugated poly(vinyl chloride) derivative, J. Alloys Compd. 1039 (2025) 183405, https://doi.org/10.1016/j.jallcom.2025.183405.

[24] J. Cao, J. He, J. Ye, K. Ge, Y. Zhang, Y. Yang, Urchin-like Bi_2S_3/Ag nanostructures for photocatalytic reduction of Cr(VI), ACS Appl. Nano Mater. 4 (2021) 1260–1269, https://doi.org/10.1021/acsanm.0c02858.

[25] S. Ma, W. Wang, Z. Hu, S. Shi, P. Yang, Y. Hou, H. Zhang, C. Chen, Z. Wang, H. Jiang, S-scheme CdS/$CuWO_4$ heterojunction optimizes reaction kinetics for enhanced photocatalytic H_2 evolution, Langmuir 42 (2026) 5156–5163, https://doi.org/10.1021/acs.langmuir.5c06431.

[26] Y.H. Ding, X.L. Zhang, N. Zhang, J.Y. Zhang, R. Zhang, Y.F. Liu, Y.Z. Fang, A visible-light driven Bi_2S_3@ZIF-8 core-shell heterostructure and synergistic photocatalysis mechanism, Dalton Trans. 47 (2018) 684–692, https://doi.org/10.1039/c7dt03256k.

[27] M. Faisal, M.A. Rashed, M.A.M. Alhmami, F.A. Harraz, Clean light oriented ultrafast Pt/Bi_2S_3 nanoflakes for the photocatalytic destruction of gemifloxacin mesylate drug and methylene blue, J. Photochem. Photobiol. A Chem. 414 (2021) 113288, https://doi.org/10.1016/j.jphotochem.2021.113288.

[28] J. Arumugam, A. George, A. Dhayal Raj, M. Selvaraj, A. Albert Irudayaraj, T. Pazhanivel, R.L. Josephine, K. Bhuvaneswari, Role of surfactant in tailoring the properties of Bi_2S_3 nanoparticles for photocatalytic degradation of methylene blue dye, J. Mater. Sci. Mater. Electron. 33 (2022) 8946–8957, https://doi.org/10.1007/s10854-021-07007-w.

[29] S. Kumaravel, C. Chandrasatheesh, G. Palanisamy, J. Lee, I. Hasan, S. Kumaravel, B. Avula, U.D. Pongiya, K. Balu, Highly efficient solar-light-active Ag-decorated g-C_3N_4 composite photocatalysts for the degradation of methyl orange dye, Micromachines 14 (2023) 1454, https://doi.org/10.3390/mi14071454.

[30] W.J. Ong, L.L. Tan, Y.H. Ng, S.T. Yong, S.P. Chai, Graphitic carbon nitride (g-C_3N_4)-based photocatalysts for artificial photosynthesis and environmental remediation: are we a step closer to achieving sustainability? Chem. Rev. 116 (2016) 7159–7329, https://doi.org/10.1021/acs.chemrev.6b00075.

[31] H.D. Tran, D.Q. Nguyen, P.T. Do, U.N.P. Tran, Kinetics of photocatalytic degradation of organic compounds: a mini-review and new approach, RSC Adv. 13 (2023) 16915–16925, https://doi.org/10.1039/d3ra01970e.

[32] S. Nasir, M.Z. Hussein, Z. Zainal, N.A. Yusof, Carbon-based nanomaterials/allotropes: a glimpse of their synthesis, properties and some applications, Materials (Basel) 11 (2018) 1–24, https://doi.org/10.3390/ma11020295.

[33] D.D. Lekeufack, A. Brioude, A. Mouti, J.G. Alauzun, P. Stadelmann, A.W. Coleman, P. Miele, Core-shell Au (TiO_2, SiO_2) nanoparticles with tunable morphology, Chem. Commun. 46 (2010) 4544–4546, https://doi.org/10.1039/c0cc00935k.

[34] Y. Xiao, H. Wang, Y. Jiang, W. Zhang, J. Zhang, X. Wu, Z. Liu, W. Deng, Hierarchical Sb_2S_3/$ZnIn_2S_4$ core–shell heterostructure for highly efficient photocatalytic hydrogen production and pollutant degradation, J. Colloid Interface Sci. 623 (2022) 109–123, https://doi.org/10.1016/j.jcis.2022.04.137.

[35] S.V. Prabhakar Vattikuti, A.K.R. Police, J. Shim, C. Byon, Sacrificiallate-free synthesis of core-shell C@Bi_2S_3 heterostructures for efficient supercapacitor and H_2 production applications, Sci. Rep. 8 (2018) 4194, https://doi.org/10.1038/s41598-018-22622-0.

[36] C. Valencia, C.H. Valencia, F. Zuluaga, M.E. Valencia, J.H. Mina, C.D. Grande-Tovar, Synthesis and application of scaffolds of chitosan-graphene oxide by the freeze-drying method for tissue regeneration, Molecules 23 (2018) 2651, https://doi.org/10.3390/molecules23102651.

[37] X. Rong, F. Qiu, J. Yan, H. Zhao, X. Zhu, D. Yang, Coupling with a narrow-band-gap semiconductor for enhancement of visible-light photocatalytic activity: preparation of Bi_2S_3/g-C_3N_4 and application for degradation of RhB, RSC Adv. 5 (2015) 24944–24952, https://doi.org/10.1039/c4ra15715j.

[38] G. Mamba, A.K. Mishra, Graphitic carbon nitride (g-C_3N_4) nanocomposites: a new and exciting generation of visible light driven photocatalysts for environmental pollution remediation, Appl. Catal. Environ. 198 (2016) 347–377, https://doi.org/10.1016/j.apcatb.2016.05.052.

[39] F.P. Ramanery, A.A.P. Mansur, H.S. Mansur, S.M. Carvalho, M.C. Fonseca, Biocompatible fluorescent core-shell nanoconjugates based on chitosan/Bi_2S_3 quantum dots, Nanoscale Res. Lett. 11 (2016) 187, https://doi.org/10.1186/s11671-016-1417-6.

[40] X. Geng, D. Zhang, Z. Zheng, G. Ye, S. Li, H. Tu, Y. Wan, P. Yang, Integrated multifunctional device based on Bi_2S_3/Pd: localized heat channeling for efficient photothermic vaporization and real-time health monitoring, Nano Energy 82 (2021) 105700, https://doi.org/10.1016/j.nanoen.2020.105700.

[41] V. NavakoteswaraRao, M.V. Shankar, B.L. Yang, C.W. Ahn, J.M. Yang, Effective excitons separation in starfish Bi_2S_3/TiO_2 nanostructures for enhanced hydrogen production, Mater. Today Chem. 26 (2022) 101096, https://doi.org/10.1016/j.mtchem.2022.101096.

[42] L. Shen, Z. Xing, J. Zou, Z. Li, X. Wu, Y. Zhang, Q. Zhu, S. Yang, W. Zhou, Black TiO_2 nanobelts/g-C_3N_4 nanosheets laminated heterojunctions with efficient visible-light-driven photocatalytic performance, Sci. Rep. 7 (2017) 41978, https://doi.org/10.1038/srep41978.

[43] J.V. Rojas, M. Toro-Gonzalez, M.C. Molina-Higgins, C.E. Castano, Facile radiolytic synthesis of ruthenium nanoparticles on graphene oxide and carbon nanotubes, Mater. Sci. Eng. B 205 (2016) 28–35, https://doi.org/10.1016/j.mseb.2015.12.005.

[44] R.I. Romanov, M.G. Kozodaev, A.G. Chernikova, I.V. Zabrosaev, A.A. Chouprik, S. S. Zarubin, S.M. Novikov, V.S. Volkov, A.M. Markeev, Thickness-dependent structural and electrical properties of WS_2 nanosheets obtained via the ALD-grown WO_3 sulfurization technique as a channel material for field-effect transistors, ACS Omega 6 (2021) 34429–34437, https://doi.org/10.1021/acsomega.1c04532.

[45] A. Hayat, M. Sohail, Z. Ajmal, H.H. Abd El-Gawad, D. Ghernaout, Y. Al-Hadeethi, S. Raza, Y. Orooji, Advances/scope and prospects of g-C_3N_4 derived fascinating photocatalyst as a leading route towards solar energy adaption, J. Clean. Prod. 438 (2024) 140568, https://doi.org/10.1016/j.jclepro.2024.140568.

[46] J.H. Thurston, N.M. Hunter, L.J. Wayment, K.A. Cornell, Urea-derived graphitic carbon nitride (u-g-C_3N_4) films with highly enhanced antimicrobial and sporicidal activity, J. Colloid Interface Sci. 505 (2017) 910–918, https://doi.org/10.1016/j.jcis.2017.06.089.

[47] F. Hassan, S.N. Backer, I.W. Almanassra, M. Ali Atieh, M. Elbahri, A. Shanableh, Solar-matched S-scheme ZnO/g-C_3N_4 for visible light-driven paracetamol degradation, Sci. Rep. 14 (2024) 12220, https://doi.org/10.1038/s41598-024-60306-0.

[48] T.M. Project, Materials Data on C_3N_4 by Materials Project, (2017). Doi: 10.17188/1313579.

[49] The Materials Data, Materials data on Bi_2S_3 by materials Project, Mater. Data (2020), https://doi.org/10.17188/1199021.

[50] R.J.C. Fernandes, A.R. Silva, B.D. Cardoso, P.J.G. Coutinho, L. Pereira, Potential of photocatalytic nanomaterials for PFOA and PFOS degradation: challenges and opportunities, J. Environ. Chem. Eng. 13 (2025) 115201, https://doi.org/10.1016/j.jece.2024.115201.

[51] R.F. Hendry, P. Needham, A.I. Woody, Introduction, in: Philos. Chem., Elsevier, 2012, pp. 3–18, https://doi.org/10.1016/B978-0-444-51675-6.50001-3.

[52] S.M. Abdel-Moniem, M.A. El-Liethy, H.S. Ibrahim, M.E.M. Ali, Innovative green/non-toxic Bi_2S_3@g-C_3N_4 nanosheets for dark antimicrobial activity and photocatalytic depollution: turnover assessment, Ecotoxicol. Environ. Saf. 226 (2021) 112808, https://doi.org/10.1016/j.ecoenv.2021.112808.

[53] A.C. Swathi, M. Chandran, Visible light responsive MWCNT decorated g-C_3N_4/Bi_2S_3 photocatalyst for malachite green dye degradation, J. Appl. Phys. 133 (2023), https://doi.org/10.1063/5.0145796.

[54] G. Palanisamy, K. Thamaraiselvi, R. Karthik, C.B. Breslin, J.-J. Shim, J. Lee, Two-dimensional titanium MXene-neodymium molybdate/tungstate/vanadate composites as efficient bifunctional catalysts for environmental remediation and hydrogen evolution reaction, Adv. Compos. Hybrid Mater. 9 (2026) 29, https://doi.org/10.1007/s42114-025-01504-w.

[55] M. Ji, J. Di, Y. Ge, J. Xia, H. Li, 2D-2D stacking of graphene-like g-C_3N_4/ultrathin $Bi_4O_5Br_2$ with matched energy band structure towards antibiotic removal, Appl. Surf. Sci. 413 (2017) 372–380, https://doi.org/10.1016/j.apsusc.2017.03.287.

[56] A.M. Basely, M.H. Shaker, F.M. Helmy, M.F. Abdel-Messih, M.A. Ahmed, Construction of Bi_2S_3/g-C_3N_4 step S-scheme heterojunctions for photothermal decomposition of rhodamine B dye under natural sunlight radiations, Inorg. Chem. Commun. 148 (2023) 110300, https://doi.org/10.1016/j.inoche.2022.110300.

[57] Z. Zhang, W. Wang, L. Wang, S. Sun, Enhancement of visible-light photocatalysis by coupling with narrow-band-gap semiconductor: a case study on Bi_2S_3/Bi_2WO_6, ACS Appl. Mater. Interfaces 4 (2012) 593–597, https://doi.org/10.1021/am2017199.

[58] D. Zhu, Q. Zhou, Nitrogen doped g-C_3N_4 with the extremely narrow band gap for excellent photocatalytic activities under visible light, Appl. Catal. Environ. 281 (2021) 119474, https://doi.org/10.1016/j.apcatb.2020.119474.



Dr. Bhuvaneswari Kandasamy is a physicist specializing in sustainable nanomaterials and environmental remediation. Her research focuses on visible-light photocatalysis, hybrid nanostructures, 3D-printed functional materials, and waste-derived materials for water and air purification. She has worked across academic and applied research settings in India and Thailand, contributing to projects in photocatalysis, electrochemical sensing, and circular-economy-based material development. Her publications and collaborative work reflect a strong interest in translating fundamental materials research into practical environmental technologies.



Dr. Balaji Parasuraman completed his doctoral degree in Physics from Periyar University. His primary research interests focus on the development of nanomaterials for electrochemical sensing and environmental applications. His research work includes the synthesis and characterization of functional nanomaterials for pollutant detection, wastewater treatment, and advanced sensing technologies. He has published research articles in reputed peer-reviewed journals and has presented his research findings at national and international conferences. His current research also emphasizes the design of efficient and sustainable materials for environmental remediation and sensor applications.



Dr. Pugazhenthiran Nalandhiran is an Assistant Professor at Universidad Técnica Federico Santa María, Chile. He earned his Ph.D. in Chemistry at Madurai Kamaraj University, India and has held research positions at Indian Institute of Technology Madras, India, Universidad de Concepción, and Universidad Católica de la Santísima Concepción, Chile. His research focuses on photocatalysis, nanostructured functional materials, hydrogen production, wastewater treatment, and sustainable energy technologies. He has authored more than 75 research articles, 6 book chapters, and has edited one book published by IOP Publishing. His publications have received over 2500 citations, with an h-index of 28. Dr. Nalandhiran actively collaborates with international researchers and is involved in several interdisciplinary projects related to clean energy, environmental remediation, and advanced materials for sustainable applications.



Dr. S. Manimegalai received her Ph.D. in Physics from Bharathidasan University. She has 14 years of teaching experience and has served at Nehru Memorial College and Vivekanandha College of Arts and Sciences for Women. She is currently working at Vivekanandha College of Engineering for Women. Her research interests include spectroscopy, nonlinear dynamics, liquid crystals, nanomaterials, and computational studies. She has published several research articles in SCI and SCI-expanded journals and has presented papers at both national and international conferences.



Dr. Sivaprakash Paramasivam completed his PhD in Physics in 2021 at Bharathidasan University, India, with a research focus on magnetic refrigeration materials and supercapacitor materials. Following his doctoral studies, he began his postdoctoral research at the Shock Wave and Gas Dynamics Laboratory, Keimyung University, South Korea. His current research primarily focuses on shock wave–material interactions and plasma treatment of materials for aerospace engineering applications.



Dr. Pazhanivel Thangavelu serves as an Assistant Professor at Periyar University, India. He completed his Ph.D. from Bharathiar University, India in 2013, focusing on the application of quantum dot materials for solar cell and explosive sensing applications. In 2015, he joined as an Assistant Professor, Periyar University and his expertise lie in environmental and sensing application. He has published more than 100 research articles in highly reputed international journals and also, he has contributed 10 book chapters in the field of nanomaterials for sensing and environmental application.



Dr. Ikhyun Kim is an Assistant Professor in the Department of Mechanical Engineering at Keimyung University, Daegu, Republic of Korea. He received his Ph.D. in Aerospace Engineering from KAIST, where his doctoral research focused on oxygen catalytic recombination phenomena investigated through shock tube experiments. He previously served as a postdoctoral researcher at the Oxford Thermofluids Institute, University of Oxford, supported by the National Research Foundation of Korea, where he conducted research on catalytic recombination and transpiration cooling in hypersonic flows. His research interests include high-speed aerothermodynamics, shock tube and tunnel facility development, heat transfer in hypersonic environments, and high-temperature materials. He has authored numerous peer-reviewed publications in leading international journals, contributing to the understanding of shock-induced surface reactions and thermal transport under extreme flow conditions.



Prof. Jintae Lee received his Ph.D. from the Department of Chemical and Biochemical Engineering at Rutgers University, USA. He is currently a full professor in the School of Chemical Engineering at Yeungnam University, Korea. He has published more than 350 peer-reviewed papers and holds over 50 patents (h-index 83). His research focuses on antimicrobial agents, bioremediation, and nanobiotechnology. He also serves as the Chair of the School of Chemical Engineering at Yeungnam University.



Dr. Govindasamy Palanisamy, born in India, received his PhD in Physics and currently works as a Research Professor, Yeungnam University, Republic of Korea. His research focuses on developing advanced hybrid materials for energy and environmental applications, including semiconductor materials, photocatalytic degradation, metal–organic frameworks, quantum dots, gas sensors, and water splitting. He has published in highly-reputed journals and continues to contribute to the scientific community through active research and editorial involvement.